chemengineering

MDPI

Article

Photocatalytic Hydrogen Production from Formic Acid Solution with Titanium Dioxide with the Aid of Simultaneous Rh Deposition

Mahmudul Hassan Suhag [1,2], Ikki Tateishi [3,*], Mai Furukawa [1], Hideyuki Katsumata [1], Aklima Khatun [1] and Satoshi Kaneco [1,*]

1 Department of Chemistry for Materials, Graduate School of Engineering, Mie University, Tsu 514-8507, Japan; suhag.che057@gmail.com (M.H.S.); maif@chem.mie-u.ac.jp (M.F.); hidek@chem.mie-u.ac.jp (H.K.); aklimarowsan_sust@yahoo.com (A.K.)
2 Department of Chemistry, University of Barishal, Barishal 8254, Bangladesh
3 Environmental Preservation Center, Mie University, Tsu 514-8507, Japan
* Correspondence: tateishi@gecer.mie-u.ac.jp (I.T.); kaneco@chem.mie-u.ac.jp (S.K.); Tel.: +81-59-231-9427 (I.T.)

Abstract: Photocatalytic hydrogen production was studied with a formic acid solution with titanium dioxide (TiO_2) with the aid of simultaneous Rh deposition. The optimum conditions were as follows: Rh loading, 0.1 wt%; formic acid concentration, 1.0%; solution, pH 2.2; temperature, 50 °C. Under the optimum conditions, the photocatalytic hydrogen production with TiO_2 by the simultaneous deposition of Rh was 5.0 mmol g^{-1}, 12.2 mmol g^{-1} and 16.0 mmol g^{-1} after 1 h, 3 h and 5 h of irradiation time for black light, respectively. Rh/TiO_2 photocatalysts were characterized by XRD, SEM, photoluminescence spectra, diffuse reflectance spectra and the BET surface area. The reaction mechanism of photocatalytic hydrogen production from formic acid by Rh/TiO_2 was also proposed.

Keywords: hydrogen production; formic acid; photocatalyst; simultaneous metal deposition; Rh/TiO_2

check for updates

Citation: Suhag, M.H.; Tateishi, I.; Furukawa, M.; Katsumata, H.; Khatun, A.; Kaneco, S. Photocatalytic Hydrogen Production from Formic Acid Solution with Titanium Dioxide with the Aid of Simultaneous Rh Deposition. *ChemEngineering* **2022**, *6*, 43. https://doi.org/10.3390/chemengineering6030043

Academic Editor: Alírio E. Rodrigues

Received: 11 March 2022
Accepted: 7 June 2022
Published: 10 June 2022

1. Introduction

In recent years, the excessive depletion of fossil fuel resources, global warming, environmental pollution and high energy demand have become serious concerns in the world [1,2]. Hence, environmentally friendly renewable energy resources, such as solar power, wind, tide, heat, biomass, geothermal, ocean, hydropower, nuclear and hydrogen energy, are needed to replace fossil fuels [3]. Hydrogen plays an important role as a renewable energy resource as a result of its unique energy storage, cleanliness, longevity, sustainability and renovation properties [3,4]. Various methods such as steam reforming, partial oxidation and the self-thermal reforming of hydrocarbons as well as fossil resources, the electrolysis of water (alkaline water electrolysis, high temperature steam electrolysis, electrolysis with a steam polymer), the pyrolysis of water, the gasification of biomass and photocatalytic water splitting have been used to produce hydrogen [3,5,6]. Steam reforming, the pyrolysis of water, the electrolysis of water and the gasification of biomass are expensive and produce carbon dioxide (CO_2) gas. Furthermore, high thermal energy is also required for these reactions. Therefore, these reactions are not appropriate for sustainable hydrogen production [3]. In contrast, only sunlight and photocatalysts are required for photocatalytic reaction. Furthermore, it can occur under ambient conditions. Hence, photocatalytic water splitting for hydrogen production has recently been the most attractive option due to its cost effective, environmentally friendly and pollution-free nature [3,6]. Several types of semiconductors as photocatalysts have been used in photocatalytic hydrogen production reaction under the irradiation of ultraviolet and visible light [3,7]. For instance, metal oxides (TiO_2, ZnO, CuO, ZrO_2, Fe_2O_3, VO_2, WO_3), chlacogenides (ZnS, CdS, CdSe), halides (AgX), carbides (SiC) and carbonaceous materials (g-C_3N_4) have been widely used for hydrogen

production by photocatalytic water splitting [2,8–17]. TiO_2 is most favorable material; it is widely used in photocatalytic hydrogen production because it is nontoxic, stable in a wide range of pH values, ecofriendly, highly photo stable and commercially available [2,5,7]. However, the main limitation of the application of TiO_2 is its lower photo activity. The recombination of charge carriers during irradiation, the occurrence of backward reaction and the fact that it is only active under UV light (4–8% of the total solar spectrum) are responsible for its lower energy conversion efficiency [2,7]. The metal/TiO_2 heterojunction decreases the charge carrier recombination and reduces the band gap energy. Hence, the heterojunction of TiO_2 and metal has been prepared by coupling the TiO_2 with metal, and it has been used as a stable and high performance photocatalyst [5,18]. The Pt, Au, Ag, Rh, Pd, Ni and Cu noble metals are coupled with TiO_2 for the enhancement of the photocatalysis reaction [1,19–23]. The photocatalytic reforming of an organic sacrificial agent solution was also used as an alternative to the photocatalysis splitting of water to increase hydrogen production. Many organic species, such as methanol, ethanol, glycerol, formic acid and ammonia borane, were used as sacrificial agents for the photocatalytic production of hydrogen [20,21,24–26]. Although Rh/TiO_2 and the sacrificial agent formic acid were individually applied to H_2 production [1,26], there is very little information on the photocatalytic hydrogen production on TiO_2 from a formic acid solution with the simultaneous photo-deposition of Rh. The present work has dealt mainly with photocatalytic H_2 production from a formic acid solution by TiO_2 with the simultaneous photo-deposition of Rh.

2. Materials and Methods

2.1. Chemicals and Materials

Photocatalyst Titanium oxide (P-25 TiO_2) was purchased from Degussa Co., Ltd., Germany (anatase 75%, rutile 25%, surface area 53 m^2 g^{-1}, particle size 25 nm). A standard stock solution of Rh^{3+} (1000 ppm) was prepared by the dissolution of $RhCl_3$ (Kanto Chemical Co., Inc., Tokyo, Japan). Sodium chloride (99.5%), formic acid (98%), sodium formate (98.0%) and ammonium formate (97.0%) were purchased from Nacalai Tesque Inc., Japan. Lithium formate (98.0%) and potassium formate (95.0%) were purchased from Wako Co., Ltd., Japan and Kanto Chemical Co., Inc., Japan, respectively. All of the chemicals were used without further purification. Pure water was obtained from an ultrapure water system (Advantec MFS Inc., Tokyo, Japan).

2.2. Photocalytic Hydrogen Production

Hydrogen generation experiments with TiO_2 powder were carried out by using simultaneous Rh deposition. The pyrex column vessel reactor (inner volume, 123 mL) was used for the photocatalytic hydrogen production from formic acid. Normally, 50 mg of the TiO_2 photocatalysts was added to 40 mL of the formic acid solution. Then, the solution containing Rh^{3+} was added to the reactor, and the concentration of Rh^{3+} was 1.25 ppm. A 15 W black lamp with an emission of about 352 nm (Toshiba Lighting & Technology Corp., Tokyo, Japan) was placed to the side of the pyrex vessel reactor as a light source. The light intensity was measured by a UV radio meter (UIT-201, Ushio Inc., Tokyo, Japan), and the value was 0.25 mW/cm^2. The TiO_2 photocatalyst was continuously stirred in the formic acid solution by a magnetic stirrer during the irradiation of light. Using a hot stirrer, the reactor temperature was kept constant at 50 °C. The reactor was sealed with a silicon septum. The irradiation time was 3 h. The generated gas was extracted from the upper part of the reactor with a microsyringe (ITO, Co., Ltd., Tokyo, Japan) and measured by gas chromatography (GL Sciences, GC-3200, Japan) with a thermal conductivity detector. The stainless column (4 m long, 2.17 mm i.d.) packed with a Molecular Sieve 5A (mesh, 60–80) was used for the separation. The carrier gas was 99.9% argon gas (Kawase Sangyo Co., Ltd., Mie, Japan). The temperature conditions of the GC were 50 °C for the injection, column and detector. The flow rate of the carrier gas was 7.0 mL/min. The analysis time and analysis sample amount were 10 min and 250 μL, respectively. The reproducibility of the

photocatalytic H_2 production test (relative standard deviation) was within an RSD of 10% for more than three of the run numbers.

2.3. Characterization of Photocatalysts

After the photocatalytic hydrogen generation experiment, the TiO_2 solution was centrifuged. Then, the supernatant and the precipitate of the Rh-deposited TiO_2 were separated, and the precipitate (Rh/TiO_2) was dried. The dried photocatalyst was crushed in an agate mortar for 15 min to obtain a photocatalyst powder. Finally, the obtained Rh-deposited TiO_2 and the pure TiO_2 were analyzed by SEM imaging, BET surface area measurement, X-ray diffraction, photoluminescence spectrum measurement and diffuse reflection spectrum measurement. X-ray powder diffraction (XRD) measurements were performed using a Rigaku RINT Ultima-IV diffractometer by Cu radiation at a scan rate of 0.04°/s in a scan range of 10–80°. The nitrogen adsorption and desorption isotherm and the Brunaure Emmett Teller (BET) specific surface area were measured by using a BEL PREP-vacIIBET surface area measuring device (MicrotracBEL Corp., Osaka, Japan). To determine the particle size of the photocatalysts, scanning electron microscope (SEM) observations were performed using a Hitachi S-4000 SEM with an accelerating voltage of 25 kV. The photoluminescence (PL) spectra of photocatalysts were observed using an RF-5300PC spectrofluorophotometer (SHIMADZU, Kyoto, Japan). The diffuse reflectance spectra of the photocatalysts were measured with a UV2450 UV-vis system (SHIMADZU, Kyoto, Japan). $BaSO_4$ was kept as a reference material in the diffuse reflectance spectra measurement.

3. Results and Discussion

3.1. Photocatalytic Hydrogen Production

3.1.1. Effect of Rh Ion Concentration

The effect of Rh ion concentration using TiO_2 with simultaneous deposition on the photocatalytic hydrogen production was investigated. The results are shown in Figure 1. It was observed that the amount of hydrogen production increased sharply with the increase in Rh^{3+} ion concentration. However, there is no dramatic change in the increase in hydrogen production after the addition of an Rh^{3+} ion concentration of 1.25 ppm. If we assume that all Rh^{3+} ions of a 1.25 ppm solution were deposited after the reaction, the Rh content on the TiO_2 photocatalyst would be 0.1 wt%. Since the trace amount of hydrogen was produced in the absence of the Rh^{3+} ions, the amount of hydrogen production was increased by about 250 times in addition to the 0.1 wt% Rh in TiO_2 with the aid of simultaneous deposition. The light filtration by the photo-deposited metal on the TiO_2 surface, the fractional blockage of the surface active site for TiO_2 in the oxidative branch at the photoreaction period and the decline in catalytic activity of the Rh/TiO_2 nanoparticle by its enlargement could be responsible for the almost constant amount of hydrogen generation at higher concentrations of Rh [20,21].

3.1.2. Effect of the Simultaneous Deposition of Rh in TiO_2

The effect of the simultaneous deposition of Rh in TiO_2 was investigated by using previously prepared Rh/TiO_2 and by simultaneously photo-depositing Rh^{3+} on TiO_2 on the photocatalytic hydrogen production from the formic acid solution. The results are shown in Figure 2. It was observed in every case that the hydrogen production from the formic acid solution by the simultaneous addition of Rh^{3+} in TiO_2 was significantly larger compared with that obtained by the prepared Rh/TiO_2 photocatalyst. The freshly deposited Rh metal on the TiO_2 surface enhanced the photocatalytic hydrogen production activity.

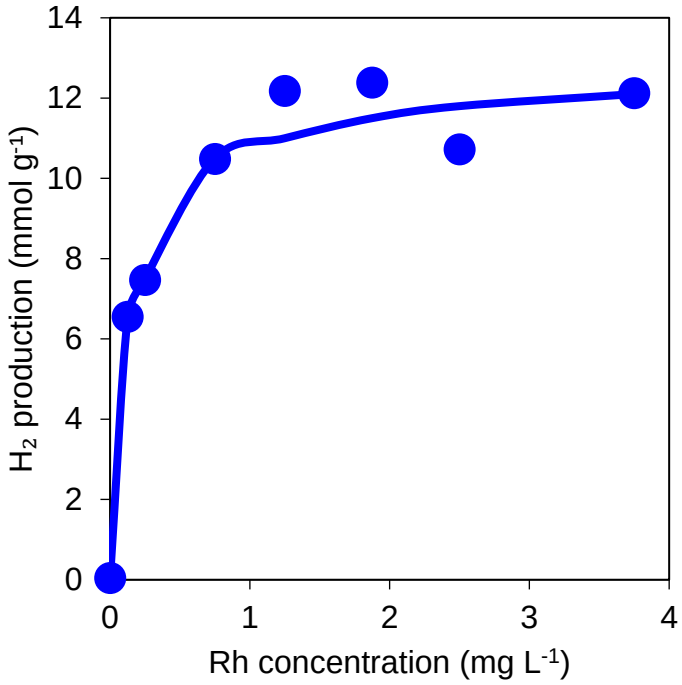

Figure 1. Effect of Rh^{3+} ion concentration. TiO_2, 50 mg; reaction time, 3 h; reaction temperature, 50 °C; formic acid concentration, 1 wt%.

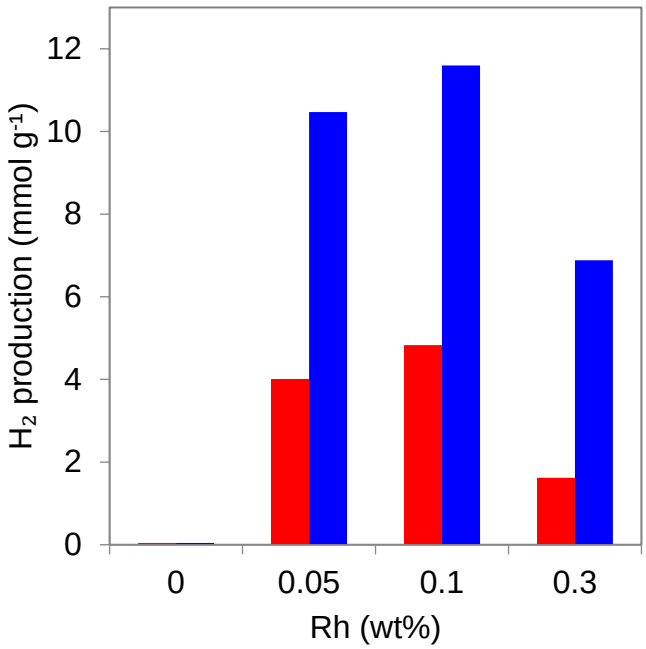

Figure 2. Comparison of the activity for the simultaneous photo-deposition of Rh in TiO_2 (blue) with the prepared Rh/TiO_2 (red). TiO_2, 50 mg; Rh, 1.25 ppm; reaction time, 3 h; reaction temperature, 50 °C; formic acid concentration, 1 wt%.

3.1.3. Effect of Formic Acid Concentration

The effect of formic acid concentration on hydrogen generation using TiO_2 with the aid of simultaneous Rh photo-deposition was investigated. The results are shown in Figure 3. It was observed that little hydrogen production occurred from the pure water. However, the photocatalytic hydrogen production increased with the increasing formic acid concentration, and the amount of hydrogen production remained almost constant in the case of using more than 1.0 wt% of formic acid. The active sites of the TiO_2 surface were

saturated with increasing formic acid concentrations, which might result in a decrease in hydrogen generation. Similar results were reported for photocatalytic hydrogen production by CuO@NiO from glycerol [27].

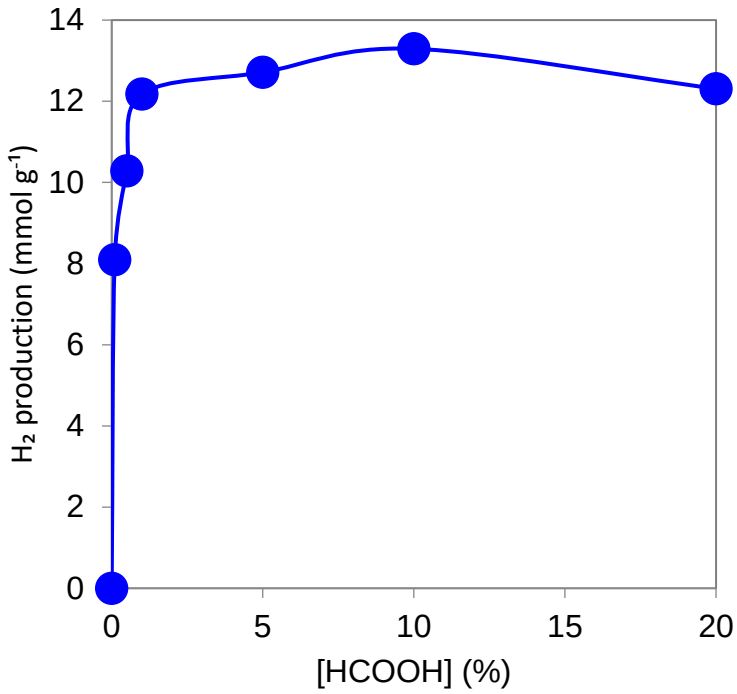

Figure 3. Effect of formic acid concentration. TiO_2, 50 mg; Rh, 1.25 ppm; reaction time, 3 h; reaction temperature, 50 °C.

3.1.4. Effect of the pH of the Reaction Solution

The effect of pH on hydrogen generation using TiO_2 with the aid of simultaneous Rh photo-deposition from a formic acid solution was investigated. The results are shown in Figure 4. It was observed that the maximum amount of hydrogen was produced (12.2 mmol g^{-1}) at pH 2.2. Moreover, the initial pH of the reaction solution containing 1.0 wt% formic acid solution was 2.2. Hence, the adjustment of the pH of the reaction solution in the subsequent experiments was unnecessary. This is because at lower pH values, more H^+ ions would be adsorbed on the surface of the TiO_2 photocatalyst, and the results were reasonable. Therefore, the reduction of the H^+ ion to H_2 was also preferred at a lower pH [28]. However, it may be partially difficult to photocatalytically deposit the Rh^{3+} ion on the TiO_2 surface at pH 1, although the chemical stability of TiO_2 could remain at pH 1.

3.1.5. Effect of Temperature

The effect of temperature on hydrogen generation using TiO_2 with the aid of simultaneous Rh photo-deposition from a formic acid solution was investigated. The results are shown in Figure 5. It was observed that the amount of hydrogen production increased with the increase in the reaction temperature. Similar results were reported for photocatalytic hydrogen production using Pt/TiO_2 at different temperatures [29]. However, 50 °C was selected as the optimum temperature, since this temperature was possible owing to the waste heat.

3.1.6. Effect of NaCl Concentration

Seawater contains sodium chloride of about 3.0 wt%. Therefore, the effect of NaCl concentration on photocatalaytic hydrogen generation using TiO_2 with the aid of simultaneous Rh deposition from a formic acid solution was inspected. It was observed that the production of hydrogen decreased with the addition of sodium chloride (Figure 6). The

dissolved chloride ion in the aqueous formic acid solution was adsorbed on the surface of the TiO_2. The chloride on the surface hindered the adsorption of formic acid on the photocatalyst [30]. Thus, the generation of hydrogen gas was disturbed by the addition of NaCl.

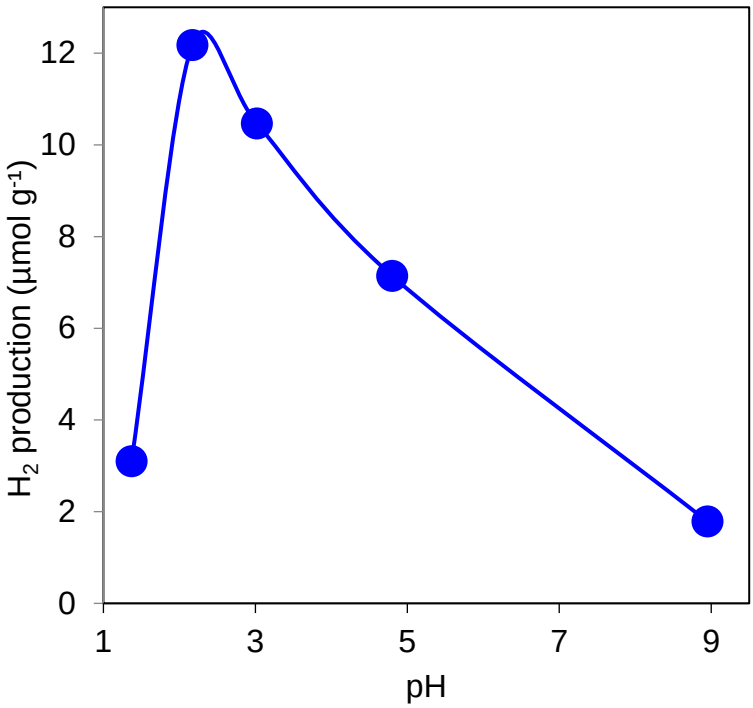

Figure 4. Effect of pH. TiO_2, 50 mg; Rh, 1.25 ppm; reaction time, 3 h; reaction temperature, 50 °C; formic acid concentration, 1 wt%.

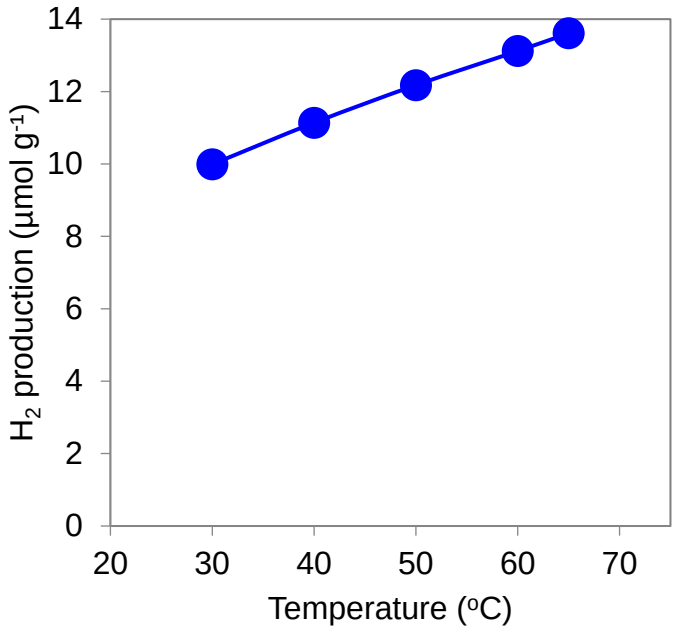

Figure 5. Effect of temperature. TiO_2, 50 mg; Rh, 1.25 ppm; reaction time, 3 h; formic acid concentration, 1 wt%.

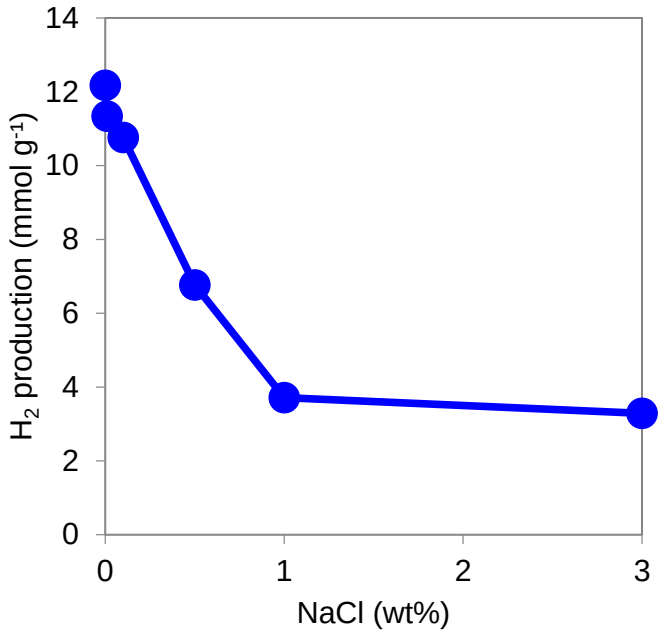

Figure 6. Effect of NaCl concentration. TiO_2, 50 mg; Rh, 1.25 ppm; reaction time, 3 h; reaction temperature, 50 °C; formic acid concentration, 1 wt%.

3.1.7. Effect of Formate Type

Various formate solutions were tested for photocatalytic hydrogen using TiO_2 with the aid of simultaneous Rh photo-deposition. Among these formates, a significant amount of hydrogen evolved from the formic acid solution (Figure 7). This result indicates that negligible amounts of hydrogen were produced from the direct hydrolysis of the formate ions ($HCOO^- + H_2O \rightarrow H_2 + HCO_3^-$) [31]. Therefore, formic acid can act as a better scavenging agent compared to ammonium formate, lithium formate, sodium formate and potassium formate.

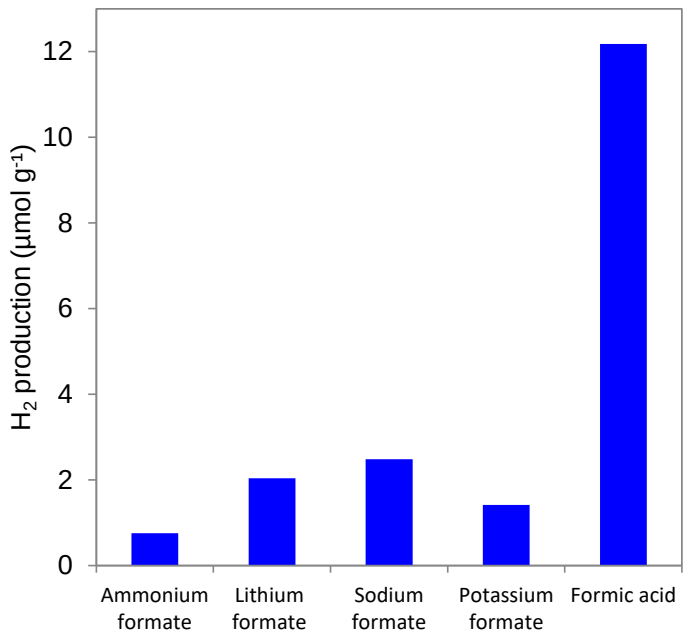

Figure 7. Effect of formate type on photocatalytic hydrogen production with TiO_2 with the aid of simultaneous Rh deposition from various formates (0.265 mol L^{-1}) and formic acid (1 wt%) solutions. TiO_2, 50 mg; Rh, 1.25 ppm; reaction time, 3 h; reaction temperature, 50 °C.

3.2. Characterization of Photocatalysts

3.2.1. XRD Analysis

The XRD of the TiO_2 and collected Rh/TiO_2 photocatalysts were analyzed. The results are shown in Figure 8. The TiO_2 photocatalyst exhibits at 2θ = 25.44°, 37.80°, 48.18°, 53.96°, 54.08°, 62.72°, 68.74°, 70.06° and 74.96°, corresponding to the (101), (004), (200), (105), (201), (204), (116), (220) and (215) planes, respectively. These peaks were observed for anatase phase of TiO_2. These results are in agreement with the previously reported work on pure TiO_2 [32]. The TiO_2 photocatalyst also exhibits peaks at 2θ = 27.42°, 36.14° and 41.34°. These three peaks could be attributed to the rutile phase of TiO_2. Similar peaks could be observed for the Rh/TiO_2 photocatalyst. Furthermore, any additional peak for the Rh/TiO_2 photocatalyst could hardly be observed. These facts indicate that the Rh metal was well dispersed on the TiO_2 crystal [33]. Hence, the crystal phase of the TiO_2 may scarcely change after the photo-deposition of the Rh metal.

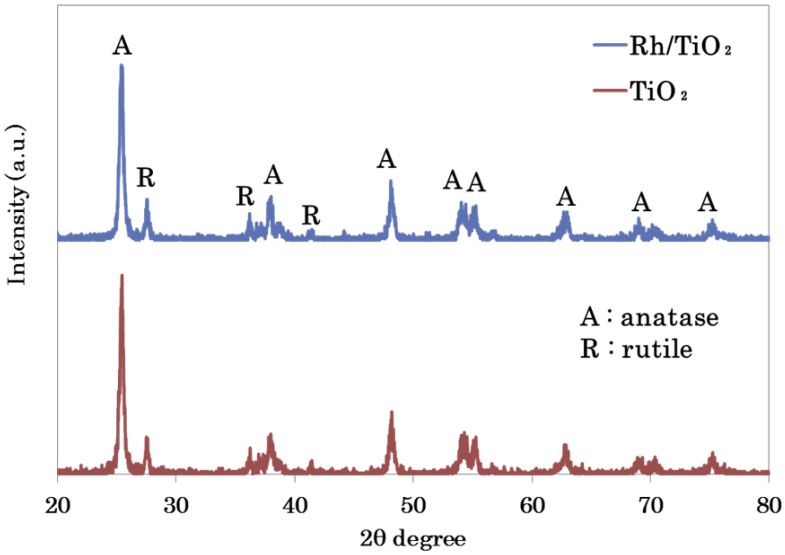

Figure 8. XRD patterns of the TiO_2 and Rh/TiO_2 photocatalysts.

3.2.2. SEM Analysis

The SEM images of both the TiO_2 and Rh/TiO_2 photocatalysts are shown in Figure 9. Figure 9A shows the spherical morphology of the TiO_2 with a particle size of 30 nm. A similar particle size and shape are also observed for the Rh/TiO_2 (Figure 9B). In the SEM image of the Rh/TiO_2 photocatalyst, the Rh particle could be hardly observed as a discrete particle, which indicated that very fine Rh particles were uniformly dispersed on the TiO_2 [4].

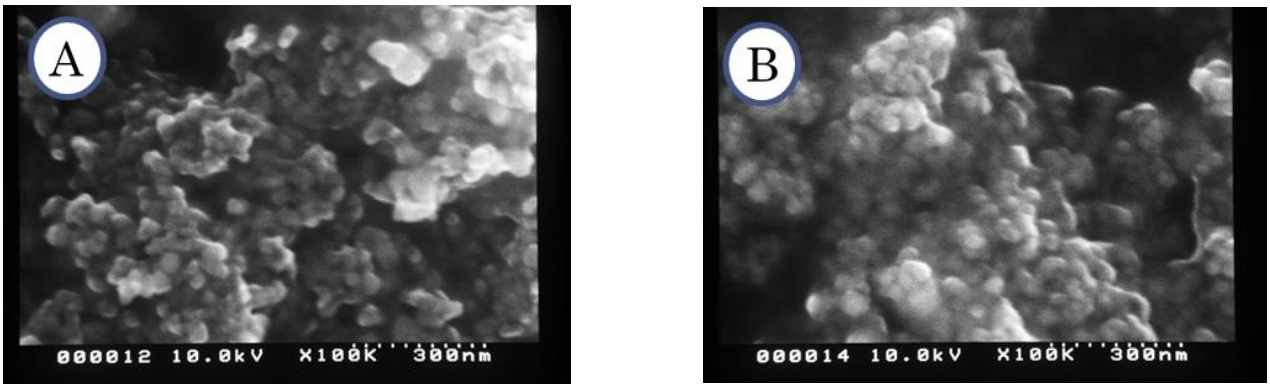

Figure 9. SEM images of TiO_2 (**A**) and Rh/TiO_2 (**B**).

3.2.3. PL Analysis

Generally, the weak fluorescence intensity is responsible for the lower recombination of the photogenerated electron hole pair. From Figure 10, it was seen that the peak intensity of the PL spectra for Rh/TiO_2 was lower than that of TiO_2, and it was observed that the photocatalytic activity of Rh/TiO_2 is greater than that of TiO_2. Thus, photogenerated carrier recombination reduction in the photo-deposition of Rh on TiO_2 was confirmed by the PL spectra [34].

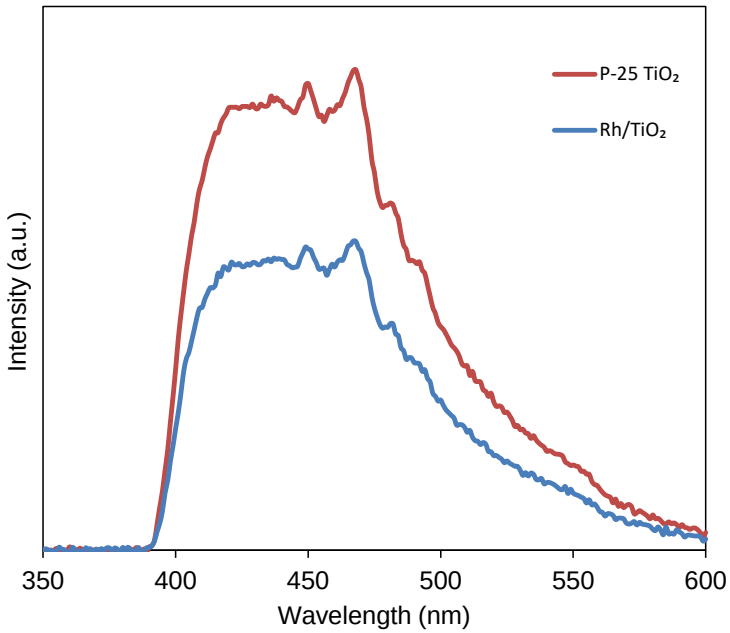

Figure 10. Photoluminescence spectra of P-25 TiO_2 and Rh/TiO_2.

3.2.4. UV–Vis Diffuse Reflection Spectrum Analysis

UV–Vis diffuse reflection spectroscopy was used to characterize the absorption edge and band gap shift of the TiO_2 before and after the photo-deposition of the Rh metal. In general, the band gap in a semiconductor is related with the absorbed wavelength, where the band gap decreases with the increase in the absorption edges [35]. The reflectance data was converted to the absorption coefficient F(R) values according to the Kubelka–Munk equation; then, the corresponding Tauc plots (plotting $\alpha h\nu$ vs. $h\nu$) were determined for the band gap energy of the photocatalysts (Figure 11) [36]. It was observed that the absorption edges of the spectra were slightly red shifted to a higher wavelength from 389 nm to 396 nm after the Rh was photo-deposited on the TiO_2. The metal doping on the TiO_2 could increase the absorption edge and decrease the band gap [4].

3.2.5. BET Surface Area

The N_2 adsorption and desorption isotherms of both photocatalysts at 77 K were measured. The results are shown in Figure 12. The isotherm of TiO_2 and Rh/TiO_2 exhibits a typical type IV isotherm, according to the classification of the adsorption and desorption isotherms by IUPAC. The results indicate that both photocatalysts were porous materials. The BET surface area, total pore volume and average pore diameter of the photocatalysts were determined from the isotherm and are presented in Table 1. It was observed that the BET surface area, total pore volume and average pore diameter of the Rh/TiO_2 increased after the photo-deposition of Rh. More photocatalytic activity for hydrogen production would be correlated with a greater BET surface area, total pore volume and average pore diameter of the photocatalyst. The photocatalytic hydrogen generation activity increased with the increase in the BET surface area and pore volume, and a decreasing pore diameter for La/TiO_2 was reported [37].

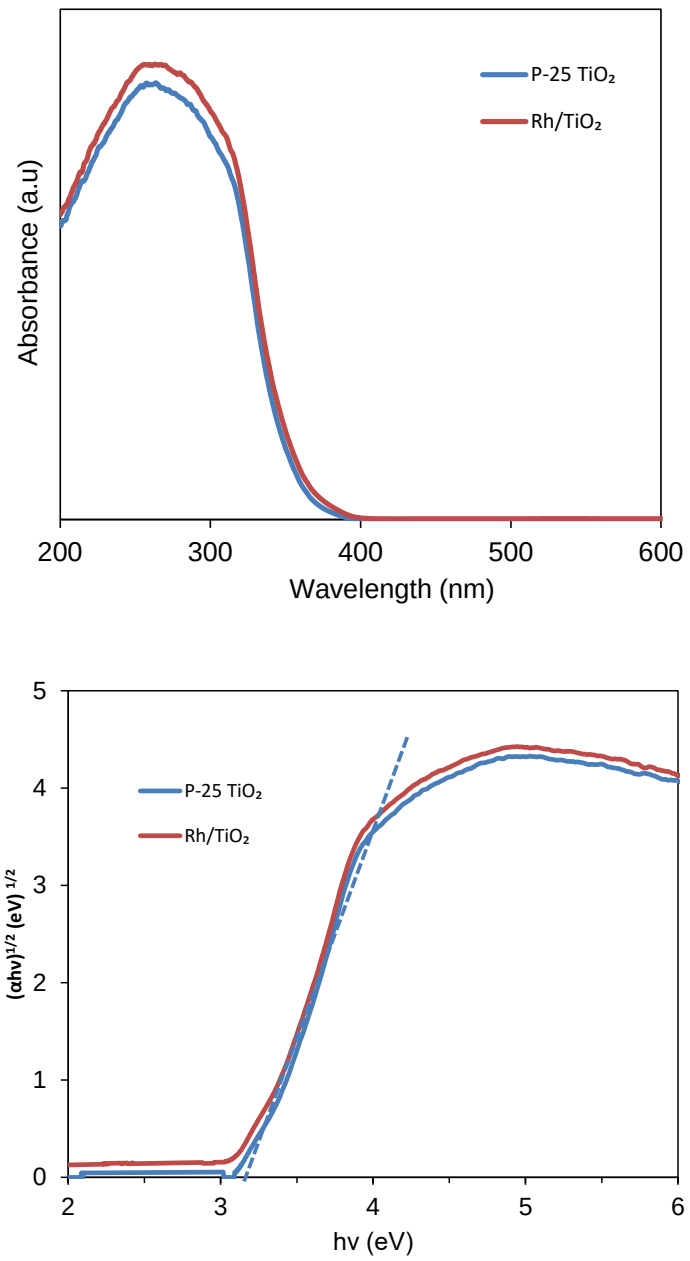

Figure 11. UV–Vis diffuse reflectance spectra (**upper**) and tauc plot (**down**) for P-25 TiO_2 and Rh/TiO_2.

3.3. Reaction Mechanism

In the present work, the photocatalytic hydrogen generation from a formic acid solution using the TiO_2 photocatalyst with the simultaneous photo-deposition of Rh metal was better relative to the hydrogen generation with bare TiO_2. On the basis of the characterization of the photocatalyst, the reasons for this may be as follows: (1) the progress of the electron-hole separation, (2) the reduction of the recombination of the electron-hole separation, (3) the metallic catalyst and (4) the slightly red shift of the absorption edge. On the basis of the experimental study in the present work and a few literature reviews of photocatalytical hydrogen generation by modified TiO_2, a possible mechanism is proposed in Figure 13 [1,5,20,21,24,26,38–40]. The pairs of the electron-hole are generated when the TiO_2 is irradiated with UV light with a wavelength of 380 nm or less. The Rh^{3+} ion is reduced to Rh metal on the TiO_2 by accepting the electrons. Furthermore, the electrons photogenerated by the TiO_2 move on the Rh. Thus, the electron-hole recombination is

reduced and stimulates the hydrogen generation reaction. On the other hand, the proton and CO_2 are generated by the oxidation of water and formate ions with photogenerated holes. Afterwards, the proton is reduced by accepting the electrons on the surface of the Rh to form hydrogen. There are two possible effects on promoting hydrogen generation in this work. Firstly, the promotion of hydrogen production on the surface of Rh metal can occur. The photogenerated electron moves from the conduction band of the TiO_2 onto the surface of the Rh metal and improves the hydrogen generation by promoting the reduction reaction of the proton. Secondly, the oxidation reaction enhances the promotion of hydrogen production. Formic acid is adsorbed on the surface of the Rh metal to promote the oxidation reaction into formaldehyde. The first effect may be considered a leading one for the increase in hydrogen generation.

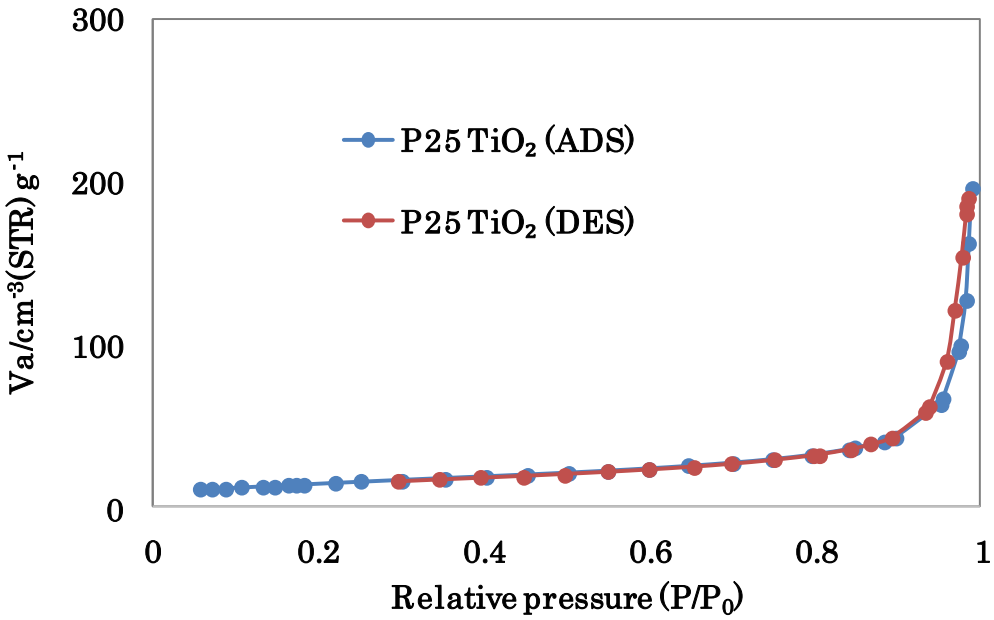

(**a**)

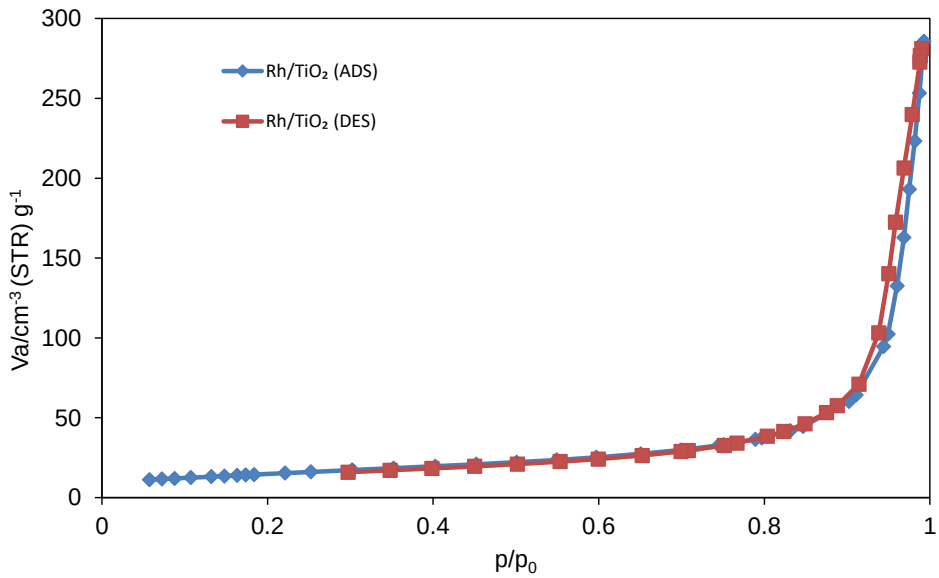

(**b**)

Figure 12. N_2 adsorption–desorption isotherms of (**a**) P-25 TiO_2 (**upper**) and (**b**) Rh/TiO_2 (**down**).

Table 1. Physicochemical properties of TiO_2 and Rh/TiO_2.

Photocatalyst	BET Surface Area [m^2 g^{-1}]	Total Pore Volume [cm^3 g^{-1}]	Average Pore Diameter [nm]
P-25 TiO_2	53	0.296	22.3
Rh/TiO_2	54	0.417	31.2

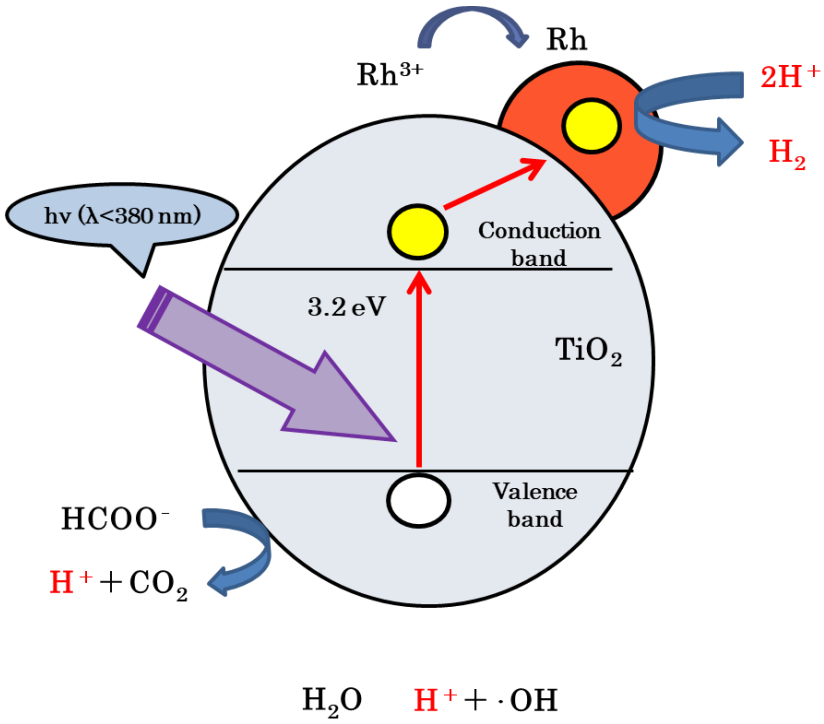

Figure 13. Photocatalytic hydrogen generation from a formic acid solution using the TiO_2 photocatalyst with the simultaneous photo-deposition of Rh.

4. Conclusions

In summary, it was found that the simultaneous photo-deposition of Rh metal on TiO_2 increased the photocatalytic hydrogen production from formic acid by TiO_2. Under optimal conditions, the photocatalytic hydrogen generation with the aid of the simultaneous photo-deposition of Rh metal on TiO_2 was about 250 times better than that obtained with the bare TiO_2.

Author Contributions: Conceptualization, M.H.S.; investigation, M.F.; data curation, M.F.; writing—original draft preparation, M.H.S. and I.T.; writing—review and editing, H.K. and A.K.; supervision, S.K. All authors have read and agreed to the published version of the manuscript.

Funding: This research was partially funded by the Grant-in-Aid for Scientific Research (B) 21H03642 from the Ministry of Education, Culture, Sports, Science, and Technology of Japan.

Data Availability Statement: Not applicable.

Acknowledgments: The authors acknowledge Kengo Minamibata for the experimental support.

Conflicts of Interest: All experiments were conducted at Mie University. Any opinions, findings, conclusions or recommendations expressed in this paper are those of the authors and do not necessarily reflect the view of the supporting organizations.

References

1. Kumaravel, V.; Mathew, S.; Bartlett, J.; Pillai, S.C. Photocatalytic hydrogen production using metal doped TiO_2: A review of recent advances. *Appl. Catal. B Environ.* **2019**, *244*, 1021–1064. [CrossRef]
2. Fiorenza, R.; Sciré, S.; D'Urso, L.; Compagnini, G.; Bellardita, M.; Palmisano, L. Efficient H_2 production by photocatalytic water splitting under UV or solar light over variously modified TiO_2-based catalysts. *Int. J. Hydrogen Energy* **2019**, *44*, 14796–14807. [CrossRef]
3. Tahir, M.; Tasleem, S.; Tahir, B. Recent development in band engineering of binary semiconductor materials for solar driven photocatalytic hydrogen production. *Int. J. Hydrogen Energy* **2020**, *45*, 15985–16038. [CrossRef]
4. Trang, T.N.Q.; Nam, N.D.; Tu, L.T.N.; Quoc, H.P.; Van Man, T.; Ho, V.T.T.; Thu, V.T.H. In Situ Spatial Charge Separation of an Ir@TiO_2 Multiphase Photosystem toward Highly Efficient Photocatalytic Performance of Hydrogen Production. *J. Phys. Chem. C* **2020**, *124*, 16961–16974. [CrossRef]
5. Leung, D.Y.C.; Fu, X.; Wang, C.; Ni, M.; Leung, M.K.H.; Wang, X.; Fu, X. Hydrogen production over titania-based photocatalysts. *ChemSusChem* **2010**, *3*, 681–694. [CrossRef] [PubMed]
6. Do, H.H.; Nguyen, D.L.T.; Nguyen, X.C.; Le, T.-H.; Nguyen, T.P.; Trinh, Q.T.; Ahn, S.H.; Vo, D.V.N.; Kim, S.Y.; Van Le, Q. Recent progress in TiO_2-based photocatalysts for hydrogen evolution reaction: A review. *Arab. J. Chem.* **2020**, *13*, 3653–3671. [CrossRef]
7. Corredor, J.; Rivero, M.J.; Rangel, C.M.; Gloaguen, F.; Ortiz, I. Comprehensive review and future perspectives on the photocatalytic hydrogen production. *J. Chem. Technol. Biotechnol.* **2019**, *94*, 3049–3063. [CrossRef]
8. Wang, S.; Zhu, B.; Liu, M.; Zhang, L.; Yu, J.; Zhou, M. Direct Z-scheme ZnO/CdS hierarchical photocatalyst for enhanced photocatalytic H_2-production activity. *Appl. Catal. B Environ.* **2019**, *243*, 19–26. [CrossRef]
9. Karthik, P.; Kumar, T.R.N.; Neppolian, B. Redox couple mediated charge carrier separation in g-C_3N_4/CuO photocatalyst for enhanced photocatalytic H_2 production. *Int. J. Hydrogen Energy* **2020**, *45*, 7541–7551. [CrossRef]
10. Wang, Q.; Edalati, K.; Koganemaru, Y.; Nakamura, S.; Watanabe, M.; Ishihara, T.; Horita, Z. Photocatalytic hydrogen generation on low-bandgap black zirconia (ZrO_2) produced by high-pressure torsion. *J. Mater. Chem. A* **2020**, *8*, 3643–3650. [CrossRef]
11. Preethi, V.; Kanmani, S. Photocatalytic hydrogen production using Fe_2O_3-based core shell nano particles with ZnS and CdS. *Int. J. Hydrogen Energy* **2014**, *39*, 1613–1622. [CrossRef]
12. Wang, Y.; Zhang, Z.; Zhu, Y.; Li, Z.; Vajtai, R.; Ci, L.; Ajayan, P.M. Nanostructured VO_2 photocatalysts for hydrogen production. *ACS Nano* **2008**, *2*, 1492–1496. [CrossRef]
13. Ye, L.; Wen, Z. $ZnIn_2S_4$ nanosheets decorating WO_3 nanorods core-shell hybrids for boosting visible-light photocatalysis hydrogen generation. *Int. J. Hydrogen Energy* **2019**, *44*, 3751–3759. [CrossRef]
14. Wang, P.; Li, H.; Sheng, Y.; Chen, F. Inhibited photocorrosion and improved photocatalytic H_2-evolution activity of CdS photocatalyst by molybdate ions. *Appl. Surf. Sci.* **2019**, *463*, 27–33. [CrossRef]
15. Mei, F.; Zhang, J.; Dai, K.; Zhu, G.; Liang, C. A Z-scheme Bi 2 MoO_6/CdSe-diethylenetriamine heterojunction for enhancing photocatalytic hydrogen production activity under visible light. *Dalt. Trans.* **2019**, *48*, 1067–1074. [CrossRef] [PubMed]
16. Hao, J.Y.; Wang, Y.Y.; Tong, X.L.; Jin, G.Q.; Guo, X.Y. Photocatalytic hydrogen production over modified SiC nanowires under visible light irradiation. *Int. J. Hydrogen Energy* **2012**, *37*, 15038–15044. [CrossRef]
17. Zhou, P.; Lv, F.; Li, N.; Zhang, Y.; Mu, Z.; Tang, Y.; Lai, J.; Chao, Y.; Luo, M.; Lin, F.; et al. Strengthening reactive metal-support interaction to stabilize high-density Pt single atoms on electron-deficient g-C_3N_4 for boosting photocatalytic H_2 production. *Nano Energy* **2019**, *56*, 127–137. [CrossRef]
18. Ni, M.; Leung, M.K.H.; Leung, D.Y.C.; Sumathy, K. A review and recent developments in photocatalytic water-splitting using TiO_2 for hydrogen production. *Renew. Sustain. Energy Rev.* **2007**, *11*, 401–425. [CrossRef]
19. Sakthivel, S.; Shankar, M.V.; Palanichamy, M.; Arabindoo, B.; Bahnemann, D.W.; Murugesan, V. Enhancement of photocatalytic activity by metal deposition: Characterisation and photonic efficiency of Pt, Au and Pd deposited on TiO_2 catalyst. *Water Res.* **2004**, *38*, 3001–3008. [CrossRef]
20. Gomathisankar, P.; Yamamoto, D.; Katsumata, H.; Suzuki, T.; Kaneco, S. Photocatalytic hydrogen production with aid of simultaneous metal deposition using titanium dioxide from aqueous glucose solution. *Int. J. Hydrogen Energy* **2013**, *38*, 5517–5524. [CrossRef]
21. Gomathisankar, P.; Kawamura, T.; Katsumata, H.; Suzuki, T.; Kaneco, S. Photocatalytic hydrogen production from aqueous methanol solution using titanium dioxide with the aid of simultaneous metal deposition. *Energy Sources Part A Recover. Util. Environ. Eff.* **2016**, *38*, 110–116. [CrossRef]
22. Tseng, I.H.; Wu, J.C.S.; Chou, H.Y. Effects of sol-gel procedures on the photocatalysis of Cu/TiO_2 in CO_2 photoreduction. *J. Catal.* **2004**, *221*, 432–440. [CrossRef]
23. Liu, S.X.; Qu, Z.P.; Han, X.W.; Sun, C.L. A mechanism for enhanced photocatalytic activity of silver-loaded titanium dioxide. *Catal. Today* **2004**, *93–95*, 877–884. [CrossRef]
24. Clarizia, L.; Spasiano, D.; Di Somma, I.; Marotta, R.; Andreozzi, R.; Dionysiou, D.D. Copper modified-TiO_2 catalysts for hydrogen generation through photoreforming of organics. A short review. *Int. J. Hydrogen Energy* **2014**, *39*, 16812–16831. [CrossRef]
25. Montini, T.; Gombac, V.; Sordelli, L.; Delgado, J.J.; Chen, X.; Adami, G.; Fornasiero, P. Nanostructured Cu/TiO_2 Photocatalysts for H_2 Production from Ethanol and Glycerol Aqueous Solutions. *ChemCatChem* **2011**, *3*, 574–577. [CrossRef]
26. Navlani-García, M.; Salinas-Torres, D.; Mori, K.; Kuwahara, Y.; Yamashita, H. *Photocatalytic Approaches for Hydrogen Production via Formic Acid Decomposition*; Springer International Publishing: Cham, Switzerland, 2019; Volume 377, ISBN 0123456789.

27. Ravi, P.; Rao, V.N.; Shankar, M.V.; Sathish, M. CuO@NiO core-shell nanoparticles decorated anatase TiO_2 nanospheres for enhanced photocatalytic hydrogen production. *Int. J. Hydrogen Energy* **2020**, *45*, 7517–7529. [CrossRef]
28. Nada, A.A.; Barakat, M.H.; Hamed, H.A.; Mohamed, N.R.; Veziroglu, T.N. Studies on the photocatalytic hydrogen production using suspended modified TiO_2 photocatalysts. *Int. J. Hydrogen Energy* **2005**, *30*, 687–691. [CrossRef]
29. Kim, G.; Choi, H.J.; Kim, H.-I.; Kim, J.; Monllor-Satoca, D.; Kim, M.; Park, H. Temperature-boosted photocatalytic H_2 production and charge transfer kinetics on TiO_2 under UV and visible light. *Photochem. Photobiol. Sci.* **2016**, *15*, 1247–1253. [CrossRef]
30. Gao, M.; Connor, P.K.N.; Ho, G.W. Plasmonic photothermic directed broadband sunlight harnessing for seawater catalysis and desalination. *Energy Environ. Sci.* **2016**, *9*, 3151–3160. [CrossRef]
31. Jiang, K.; Xu, K.; Zou, S.; Cai, W. B-Doped Pd Catalyst: Boosting Room-Temperature Hydrogen Production from Formic Acid—Formate Solutions. *J. Am. Chem. Soc.* **2014**, *136*, 4861–4864. [CrossRef]
32. Swapna, M.V.; Haridas, K.R. An easier method of preparation of mesoporous anatase TiO_2 nanoparticles via ultrasonic irradiation. *J. Exp. Nanosci.* **2016**, *11*, 540–549. [CrossRef]
33. Camposeco, R.; Hinojosa-Reyes, M.; Zanella, R. Highly efficient photocatalytic hydrogen evolution by using Rh as co-catalyst in the Cu/TiO_2 system. *Int. J. Hydrogen Energy* **2021**, *46*, 26074–26086. [CrossRef]
34. Duan, S.; Zhang, S.; Chang, S.; Meng, S.; Fan, Y.; Zheng, X.; Chen, S. Efficient photocatalytic hydrogen production from formic acid on inexpensive and stable phosphide/$Zn_3In_2S_6$ composite photocatalysts under mild conditions. *Int. J. Hydrogen Energy* **2019**, *44*, 21803–21820. [CrossRef]
35. Wang, Q.; An, N.; Bai, Y.; Hang, H.; Li, J.; Lu, X.; Liu, Y.; Wang, F.; Li, Z.; Lei, Z. High photocatalytic hydrogen production from methanol aqueous solution using the photocatalysts CuS/TiO_2. *Int. J. Hydrogen Energy* **2013**, *38*, 10739–10745. [CrossRef]
36. Chen, W.-T.; Chan, A.; Sun-Waterhouse, D.; Moriga, T.; Idriss, H.; Waterhouse, G.I.N. Ni/TiO_2: A promising low-cost photocatalytic system for solar H_2 production from ethanol-water mixtures. *J. Catal.* **2015**, *326*, 43–53. [CrossRef]
37. Tahir, M. La-modified TiO_2/carbon nanotubes assembly nanocomposite for efficient photocatalytic hydrogen evolution from glycerol-water mixture. *Int. J. Hydrogen Energy* **2019**, *44*, 3711–3725. [CrossRef]
38. Ma, Y.; Wang, X.; Jia, Y.; Chen, X.; Han, H.; Li, C. Titanium dioxide-based nanomaterials for photocatalytic fuel generations. *Chem. Rev.* **2014**, *114*, 9987–10043. [CrossRef]
39. Halasi, G.; Schubert, G.; Solymosi, F. Photodecomposition of formic acid on N-doped and metal-promoted TiO_2 production of CO-free H_2. *J. Phys. Chem. C* **2012**, *116*, 15396–15405. [CrossRef]
40. Gupta, B.; Melvin, A.A.; Matthews, T.; Dash, S.; Tyagi, A.K. TiO_2 modification by gold (Au) for photocatalytic hydrogen (H_2) production. *Renew. Sustain. Energy Rev.* **2016**, *58*, 1366–1375. [CrossRef]